Reprinted from

APPLIED PHYSICS EXPRESS

Spin-Torque Diode Measurements of MgO-Based Magnetic Tunnel Junctions with Asymmetric Electrodes

Rie Matsumoto, André Chanthbouala, Julie Grollier, Vincent Cros, Albert Fert, Kazumasa Nishimura, Yoshinori Nagamine, Hiroki Maehara, Koji Tsunekawa, Akio Fukushima, and Shinji Yuasa

Appl. Phys. Express **4** (2011) 063001

Applied Physics Express 4 (2011) 063001
DOI: 10.1143/APEX.4.063001

Spin-Torque Diode Measurements of MgO-Based Magnetic Tunnel Junctions with Asymmetric Electrodes

Rie Matsumoto*, André Chanthbouala, Julie Grollier, Vincent Cros, Albert Fert, Kazumasa Nishimura[1], Yoshinori Nagamine[1], Hiroki Maehara[1], Koji Tsunekawa[1], Akio Fukushima[2], and Shinji Yuasa[2]

Unité Mixte de Physique CNRS/Thales and Université Paris Sud 11, 91767 Palaiseau Cedex, France
[1]*Process Development Center, Canon ANELVA Corporation, Kawasaki 215-8550, Japan*
[2]*National Institute of Advanced Industrial Science and Technology (AIST), Spintronics Research Center, Tsukuba, Ibaraki 305-8568, Japan*

Received February 27, 2011; accepted April 12, 2011; published online May 17, 2011

We present a detailed study of the spin-torque diode effect in CoFeB/MgO/CoFe/NiFe magnetic tunnel junctions. From the evolution of the resonance frequency with magnetic field at different angles, we clearly identify the free-layer mode and find an excellent agreement with simulations by taking into account several terms for magnetic anisotropy. Moreover, we demonstrate the large contribution of the out-of-plane torque in our junctions with asymmetric electrodes compared to the in-plane torque. Consequently, we provide a way to enhance the sensitivity of these devices for the detection of microwave frequency. © 2011 The Japan Society of Applied Physics

Spin-transfer torque (STT) in MgO-based magnetic tunnel junctions (MTJs)[1,2] is under development for device applications such as STT random access memories (STT-RAM),[3,4] domain-wall-motion MRAM,[5] racetrack memory[6] and spintronic memristors.[7,8] Recently, spin-torque diodes[9] have attracted much attention because their sensitivity for the detection of microwave frequency may exceed that of semiconductor diodes.[10,11] In the spin diode effect, an applied rf current to the MTJ exerts an oscillating spin torque on the magnetization of the free layer, leading to excitation of the ferromagnetic resonance (FMR) mode. The dynamics of the free layer cause oscillations of the tunnel magnetoresistance (TMR). As a result, the oscillating resistance partially rectifies the rf current and dc voltage is obtained (V_{diode}). The spin diode effect depends on the relative amplitudes (a_J and b_J) of the classical in-plane torque ($\mathbf{T}_{\mathrm{IP}}$) and the out-of-plane field-like torque ($\mathbf{T}_{\mathrm{OOP}}$).[12,13] Here, the torques are expressed as $\mathbf{T}_{\mathrm{IP}} = -\gamma(a_J/M_s)\mathbf{m}\times(\mathbf{m}\times\mathbf{M}_{\mathrm{ref}})$ and $\mathbf{T}_{\mathrm{OOP}} = -\gamma b_J \mathbf{m}\times\mathbf{M}_{\mathrm{ref}}$ with $\mathbf{m}$ (M_s) being the magnetization vector (the saturation magnetization) of the free layer, $\mathbf{M}_{\mathrm{ref}}$ the magnetization vector of the reference layer, and γ the gyromagnetic ratio. In spin diode spectra [V_{diode} as a function of frequency (f)], the contribution of $\mathbf{T}_{\mathrm{IP}}$ (and $\mathbf{T}_{\mathrm{OOP}}$) results in a peak with a Lorentzian component (and an anti-Lorentzian component, respectively);

$$V_{\mathrm{diode}} = \frac{A(f_1^2 - f^2) + Bf^2}{(f_1^2 - f^2)^2 + (\Delta f)^2}, \tag{1}$$

$$A \propto \gamma^2 H_{\mathrm{d}} \frac{\partial b_J}{\partial I} \mathrm{TMR}\sin^2\theta, \tag{2}$$

$$B \propto \gamma\Delta \frac{\partial a_J}{\partial I} \mathrm{TMR}\sin^2\theta, \tag{3}$$

where A and B are the amplitudes of the anti-Lorentzian and Lorentzian components, respectively, f_1 is the resonance frequency, and Δ is the peak linewidth. In the macrospin approximation using the assumption that the free-layer magnetization is aligned along the hard axis direction, a macrospin model leads to eqs. (2) and (3) for the parameters A and B.[14] H_{d} is the out-of-plane demagnetization field, I is the bias dc current, and θ is the relative angle between the free and reference layers. The experimentally evaluated

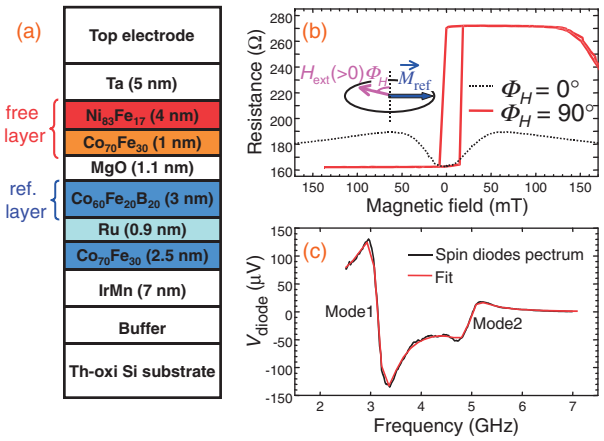

Fig. 1. (a) Sketch of the MgO-based magnetic tunnel junction (MTJ) stack. (b) Resistance versus magnetic field curves obtained for the in-plane magnetic field applied along 0° (dotted line) and 90° (solid line). Inset in (b) is a schematic explaining our convention of the angle (ϕ_{H}) of the in-plane magnetic field (H_{ext}) and the magnetization direction of the reference layer (M_{ref}). (c) Spin-torque diode signal (V_{diode}) versus frequency measured under $H_{\mathrm{ext}} = +20$ mT with $\phi_{\mathrm{H}} = 0°$ with fitted curve.

$\mathbf{T}_{\mathrm{OOP}}$ was reported to reach over 25% of $\mathbf{T}_{\mathrm{IP}}$ in conventional CoFeB/MgO/CoFeB MTJs with symmetric electrodes.[12,13] However, in these MTJs, the dc bias dependence of $\mathbf{T}_{\mathrm{OOP}}$ is quadratic and symmetric with respect to the polarity of bias, leading to $A = 0$ at zero dc bias voltage. For MTJs with asymmetric electrodes, on the other hand, the bias dependence of $\mathbf{T}_{\mathrm{OOP}}$ is expected to be asymmetric and linear at low bias,[15,16] leading to a larger A at zero dc bias voltage. In this study, we perform spin diode measurements of MgO-based MTJs with asymmetric electrodes. We also measure its dependence on the magnitude and angle of the in-plane external magnetic field (H_{ext}) to identify the free-layer excitation modes.

Thin films of MTJs are deposited with a magnetron sputtering system (Canon ANELVA C-7100). The stacking structure [see Fig. 1(a)] is IrMn (7)/$Co_{70}Fe_{30}$ (2.5)/Ru (0.9)/$Co_{60}Fe_{20}B_{20}$ (3)/MgO tunnel barrier (1.1)/$Co_{70}Fe_{30}$ (1)/$Ni_{83}Fe_{17}$ (4)/capping layers (thickness in nm) deposited on thermally oxidized Si substrate/buffer layers. Annealing treatment in a high-vacuum furnace at 330 °C for 2 h is then carried out under a 1 T magnetic field.

*E-mail address: rie.matsumoto@thalesgroup.com

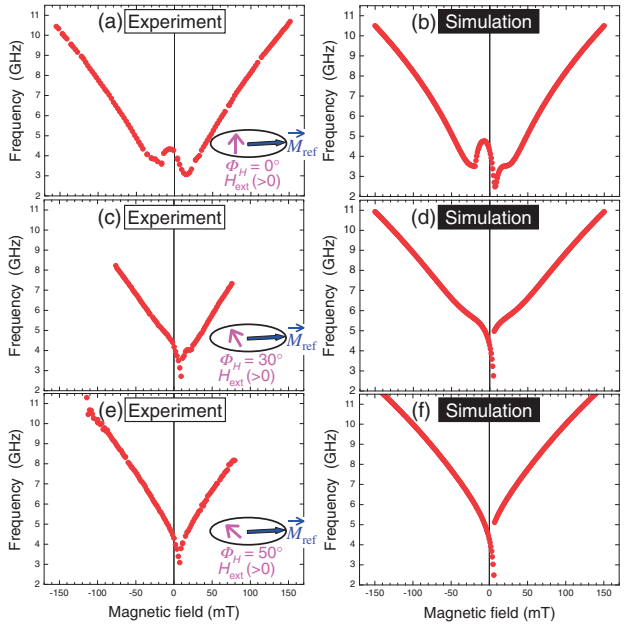

Fig. 2. Resonance frequency of the free-layer mode versus the external magnetic field (H_{ext}) with various angles (f) of (a, b) 0°, (c, d) 30°, and (e, f) 50°. (a, c, e) Experimental results. Insets in (a)–(c) are schematics explaining our convention of the angle (ϕ_H) of the in-plane magnetic field (H_{ext}) and the magnetization direction of the reference layer (M_{ref}). (b, d, f) Simulation results with consistent parameters: in-plane shape-anisotropy field (H_{SA}) of 20 mT, in-plane crystalline-anisotropy field (H_{CA}) of 10 mT, angle of crystalline-anisotropy field in CoFe layer (β) of 63°, and $H_d = 1.1$ T.

These MTJ films are micro processed into nano pillars with an elliptic junction area of $70 \times 270\,\text{nm}^2$. All the measurements presented here were carried out at room temperature. We first present in Fig. 1(b) the resistance versus magnetic field [$R(H)$] curves obtained for in-plane H_{ext} applied along 0 and 90° [the definition of the angle for H_{ext} (ϕ_H) is schematically shown in the inset of Fig. 1(b)]. The TMR ratio is 67.7% and the resistance is 162 Ω in the parallel magnetic state. The angular spin diode measurements presented in the following are performed with in-plane H_{ext} at various ϕ_H. The injected microwave power is kept constant at −15 dBm, and no dc current is applied.

As an example of spin diode measurements, in Fig. 1(c) we show the spectrum obtained at $H_{ext} = +20$ mT with $\phi_H = 0°$. In the MTJs of this study, the spin diode spectrum typically has two peaks that we label Mode 1 and Mode 2. As expected from eq. (2), in the case of the MTJs with asymmetric electrodes, the peaks have a significant anti-Lorentzian component. The peaks are well fitted by eq. (1) [see Fig. 1(c)].

First, we focus on the property of Mode 1. The resonance frequency of Mode 1 versus H_{ext} [$f_1(H)$] at different angles is shown in Figs. 2(a), 2(c), and 2(e). For higher $|H_{ext}| > 50$ mT, $f_1(H)$ increases with increasing H_{ext} following the Kittel formula.[17] Fitting $f_1(H)$ for $\phi_H = 0°$ with the Kittel formula gives $H_d = 1.1$ T. For small $H_{ext} < 50$ mT, $f_1(H)$ exhibits an asymmetric behavior with respect to the polarity of H_{ext}, especially for H_{ext} with $\phi_H = 0°$ [Fig. 2(a)]. This characteristic cannot be explained by the macro-spin model taking into account only the in-plane shape-anisotropy field (H_{SA}). The in-plane crystalline-anisotropy field (H_{CA}) due to $Co_{70}Fe_{30}$ in the free layer can be responsible for this asymmetric $f_1(H)$. The CoFe layer is amorphous in the as-grown state but it crystallizes in a cubic-crystal texture by post-annealing[4] then leading to cubic anisotropy. It should be noted that its in-plane crystalline orientation can be arbitrary.

To understand this asymmetric $f_1(H)$, we analytically simulate the resonance frequency versus H_{ext} of the free layer [$f_{free}(H)$] with the macro-spin model taking into account not only H_{SA} but also the fourfold H_{CA}[18] due to $Co_{70}Fe_{30}$ having an arbitrary crystalline orientation. First, the equilibrium angle of the free-layer magnetization (ϕ) under H_{ext} with ϕ_H is given by

$$H_{ext}\sin(\phi - \phi_H) = \frac{1}{2}H_{SA}\sin 2\phi - \frac{1}{4}H_{CA}\cos 4(\phi - \beta). \quad (4)$$

Here, β is the angle of crystalline easy axis in the CoFe layer, defined with respect to the minor axis of the patterned ellipse. Then, $f_{free}(H)$ is given by

$$f = \frac{\gamma}{2\pi}\{H_d[H_{ext}\cos(\phi - \phi_H) - H_{SA}\cos 2\phi + H_{CA}\cos 4(\phi - \beta)]\}^{1/2}. \quad (5)$$

The simulation results are shown in Figs. 2(b), 2(d), and 2(f). Here, we fix all the parameters except for H_{ext} and ϕ_H : $H_{SA} = 20$ mT, $H_{CA} = 10$ mT, $\beta = 63°$, and $H_d = 1.1$ T. The qualitative correspondence between the analytically simulated $f_{free}(H)$ and experimental $f_1(H)$ indicates that Mode 1 corresponds to the free-layer mode, and that the contribution of H_{CA} is not negligible.

We also measure $f_1(H)$ of other samples on the same lot. Although each sample exhibits the asymmetric $f_1(H)$ with a different characteristic at $\phi_H = 0°$, each $f_1(H)$ can be qualitatively explained by eqs. (3) and (4) with various β (0–90°), similar values of H_{SA} (20–40 mT) and H_{CA} (15–20 mT), and the same $H_d = 1.1$ T. This result also supports the measurable contribution of H_{CA}. To further obtain quantitative agreement between the simulated $f_{free}(H)$ and experimental $f_1(H)$, especially in the low-field range, we need to take into account the coupling with Mode 2. However, the origin of Mode 2 is still under debate, while such higher-order modes are often observed in MgO-based MTJs. Depending on the authors, the origin is attributed to the edge mode, higher-order spin wave mode, or mode of CoFe/Ru/CoFeB synthetic antiferromagnetic layers.[10,19] To discuss the origin of Mode 2 is beyond the scope of this letter.

The fitting parameters A (anti-Lorentzian component) and B (Lorentzian component) of eq. (1) versus H_{ext} with $\phi_H = 0°$ that maximizes the spin diode effect are shown in Figs. 3(a) and 3(b), respectively. First, the amplitude of the parameter A is one order of magnitude larger than that of the parameter B. Indeed, from eqs. (2) and (3), it appears that parameter A is proportional to large γH_d whereas parameter B is proportional to a small $\Delta \approx \gamma\alpha H_d$, where α is the Gilbert damping.[12–14] This model, which relies on the assumption that the free-layer magnetization is saturated along the hard axis, is applicable only to the field amplitudes larger than 60 mT in our experiment (corresponding to the colored box surrounded by doted lines in Fig. 3). In this range, the average value of A/B is larger than 50. The linear

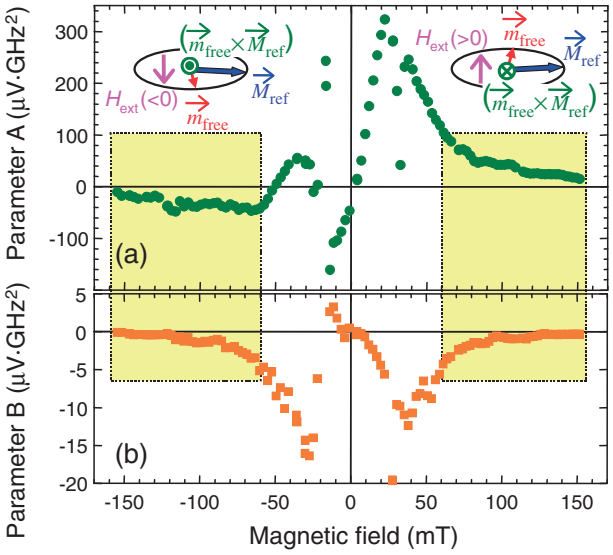

Fig. 3. Magnetic field dependence of (a) fitting parameter A and (b) fitting parameter B of eq. (1). Insets in (a) are schematics explaining our convention of the angle (ϕ_H) of the in-plane magnetic field (H_{ext}) and the magnetization directions of the free (m_{free}) and reference (M_{ref}) layers. The colored boxes indicate the range of the validity of eqs. (2) and (3).

bias dependence of $\mathbf{T}_{OOP}$ in the MTJs with asymmetric electrodes might open a way to enhance the diode sensitivity (V_{diode} divided by the injected rf power).

We also check the diode sensitivity with a similar sample on the same lot. Here, we carefully measure the bias dc dependence of resistance and the diode effect,[8] and calibrate the impedance mismatch of the sample using the measured bias dependence of the resistance and backgrounds of the spin diode spectra.[14] At $H_{ext} = 42\,\mathrm{mT}$, we obtain a diode sensitivity of 100 mV/mW. This sensitivity is competitive compared to those of past studies although the TMR ratio in our study is about half.[10,11]

For higher $|H_{ext}| > 60\,\mathrm{mT}$, parameter A changes its sign depending on the polarity of H_{ext} while the sign of parameter B is independent of the polarity of H_{ext}. This result agrees with the vectorial expression of the spin torques because the vector product in $\mathbf{T}_{OOP}$ changes polarity depending on the polarity of H_{ext} as schematically shown in the insets of Fig. 3, while the vector product in $\mathbf{T}_{IP}$ does not. The above-mentioned characteristics of the H_{ext} dependence of parameters A and B also support that Mode 1 corresponds to the free-layer mode.

In summary, spin diode measurements are performed in CoFeB/MgO/CoFe/NiFe MTJs having asymmetric electrodes without dc bias current. Their spin diode spectra exhibit peaks with strong anti-Lorentzian components originating from $\mathbf{T}_{OOP}$ in the asymmetric MTJs. Because of the significant contribution of $\mathbf{T}_{OOP}$, under an in-plane magnetic field of 42 mT, we obtain a diode sensitivity as large as 100 mV/mW (after impedance matching correction). We also perform the spin diode measurements under various H_{ext} with ϕ_H. By comparing the experimental $f_1(H)$ with the simulation results of $f_{free}(H)$, we can identify the free-layer excitation modes where the contribution of H_{CA} is observed to be measurable as well as H_{SA}.

Acknowledgments This work was supported by the European Research Council (ERC Stg 2010 No. 259068) and JSPS Postdoctoral Fellowships for Research Abroad.

1) S. S. P. Parkin, C. Kaiser, A. Panchula, P. M. Rice, B. Hughes, M. Samant, and S.-H. Yang: Nat. Mater. **3** (2004) 862.
2) S. Yuasa, T. Nagahama, A. Fukushima, Y. Suzuki, and K. Ando: Nat. Mater. **3** (2004) 868.
3) M. Hosomi, H. Yamagishi, T. Yamamoto, K. Bessho, Y. Higo, K. Yamane, H. Yamada, M. Shoji, H. Hachino, C. Fukumoto, H. Nagao, and H. Kano: IEDM Tech. Dig., 2005, p. 459.
4) S. Yuasa and D. D. Djayaprawira: J. Phys. D **40** (2007) R337.
5) S. Fukami, T. Suzuki, K. Nagahara, N. Ohshima, Y. Ozaki, S. Saito, R. Nebashi, N. Sakimura, H. Honjo, K. Mori, C. Igarashi, S. Miura, N. Ishiwata, and T. Sugibayashi: VLSI Tech. Dig., 2009, p. 230.
6) S. S. P. Parkin, M. Hayashi, and L. Thomas: Science **320** (2008) 190.
7) X. Wang, Y. Chen, H. Xi, H. Li, and D. Dimitrov: IEEE Electron Device Lett. **30** (2009) 294.
8) A. Chanthbouala, R. Matsumoto, J. Grollier, V. Cros, A. Anane, A. Fert, A. V. Khvalkovskiy, K. A. Zvezdin, K. Nishimura, Y. Nagamine, H. Maehara, K. Tsunekawa, A. Fukushima, and S. Yuasa: arXiv:1102.2106v1; to be published in Nat. Phys.
9) A. A. Tulapurkar, Y. Suzuki, A. Fukushima, H. Kubota, H. Maehara, K. Tsunekawa, D. D. Djaraprawira, N. Watanabe, and S. Yuasa: Nature **438** (2005) 339.
10) C. Wang, Y.-T. Cui, J. Z. Sun, J. A. Katine, R. A. Buhrman, and D. C. Ralph: J. Appl. Phys. **106** (2009) 053905.
11) S. Ishibashi, T. Seki, T. Nozaki, H. Kubota, S. Yakata, A. Fukushima, S. Yuasa, H. Maehara, K. Tsunekawa, D. D. Djayaprawira, and Y. Suzuki: Appl. Phys. Express **3** (2010) 073001.
12) H. Kubota, A. Fukushima, K. Yakushiji, T. Nagahama, S. Yuasa, K. Ando, H. Maehara, Y. Nagamine, K. Tsunekawa, D. D. Djayaprawira, N. Watanabe, and Y. Suzuki: Nat. Phys. **4** (2008) 37.
13) J. C. Sankey, Y.-T. Cui, J. Z. Sun, J. C. Slonczewski, R. A. Buhrman, and D. C. Ralph: Nat. Phys. **4** (2008) 67.
14) C. Wang, Y.-T. Cui, J. Z. Sun, J. A. Katine, R. A. Buhrman, and D. C. Ralph: Phys. Rev. B **79** (2009) 224416.
15) J. Xiao, G. E. W. Bauer, and A. Brataas: Phys. Rev. B **77** (2008) 224419.
16) S.-C. Oh, S.-Y. Park, A. Manchon, M. Chshiev, J.-H. Han, H.-W. Lee, J.-E. Lee, K.-T. Nam, Y. Jo, Y.-C. Kong, B. Dieny, and K.-J. Lee: Nat. Phys. **5** (2009) 898.
17) C. Kittel: *Introduction to Solid State Physics* (Wiley, New York, 1996) 7th ed., p. 505.
18) Yu. V. Goryunov, N. N. Garif'yanov, G. G. Khaliullin, I. A. Garifullin, L. R. Tagirov, F. Schreiber, Th. Mühge, and H. Zabel: Phys. Rev. B **52** (1995) 13450.
19) A. Helmer, S. Cornelissen, T. Devolder, J.-V. Kim, W. van Roy, L. Lagae, and C. Chappert: Phys. Rev. B **81** (2010) 094416.